Supporting Information:

E-mail:

Contents

1 Detailed Experimental Methods

1.1 Metal-cation precursors

Metal-cation precursors used included: nickel(II) chloride anhydrous, Alfa Aesar B22085; potassium tetrachloroplatinate(II), Alfa Aesar 11048; ruthenium(III) chloride hydrate, Sigma-Aldrich 206229; molybdenum(III) chloride, Beantown Chemical 132345; potassium tetrachloropalladate(II), Beantown Chemical 129355; lead(II) chloride, Sigma-Aldrich 268690; tin(II) chloride dihydrate, Fisher Scientific S25578; silver trifluoromethanesulfonate, Alfa Aesar, 88722; aluminum trifluoromethanesulfonate, Oakwood Chemical, 003954; gold(III)

chloride, Strem Chemical, 93-7907; bismuth(II) chloride, TCI, B3546; cobalt(II) chloride, Alfa Aesar, B22031; chromium(III) chloride hexahydrate, Strem Chemical, 93-2417; europium(III) chloride hexahydrate, Sigma-Aldrich, 203254; iron(II) chloride tetrahydrate, Sigma-Aldrich, 22,029-9; gallium nitrate hydrate, Alfa Aesar, 11150; indium(I) chloride, Alfa Aesar, 40033; iridium(III) chloride hydrate, J&J Materials, 408828; lanthanum(III) chloride, Strem Chemical, 93-5708; lithium chloride, Acros, 199881000; manganese(II) chloride, Beantown Chemical, 137725; osmium(III) chloride hydrate, Acros, 318705000; rhodium(III) chloride hydrate, Thermo-Fischer, 900030512; vanadium(III) chloride, Strem Chemical, 23-4300; and zinc chloride, Alfa Aesar, 87900.

2 Supplemental Figures

2.1 Volcano Plots in Various Media

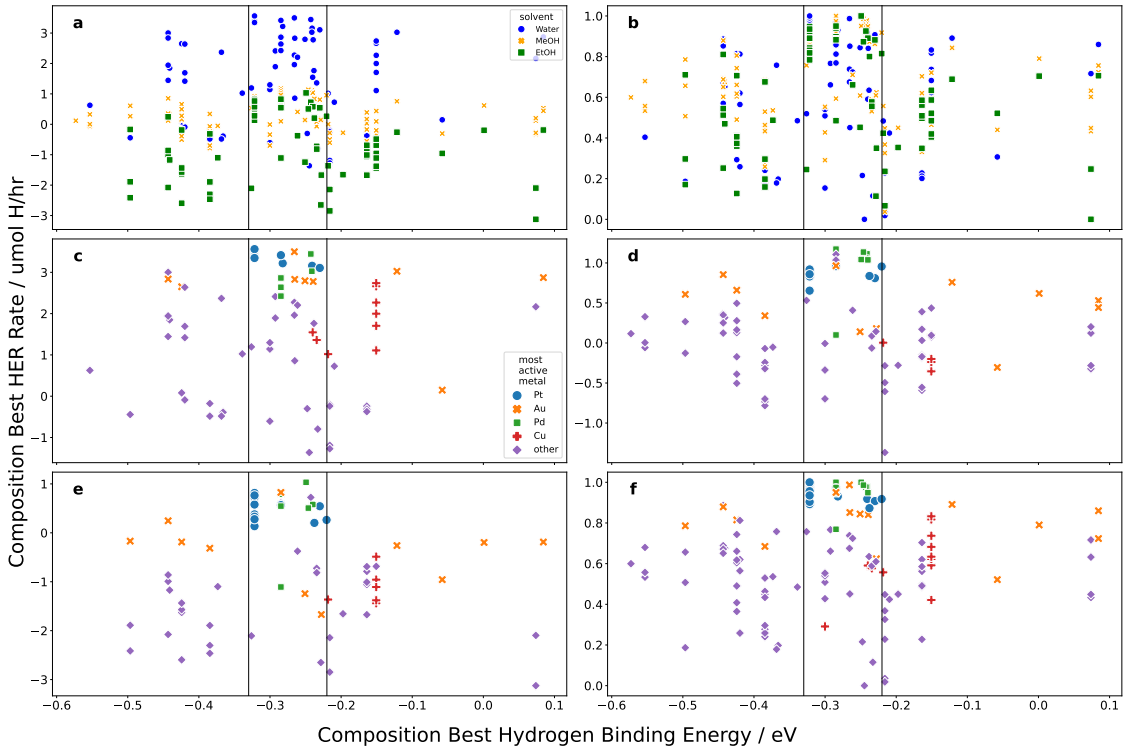

Figure S1: Volcano plots constructed by plotting the low-coverage hydrogen binding energy of the most active surface (i.e. the surface with a low-coverage binding energy closest to -0.24 eV) against the highest HER rate observed over all experiments for each chemical composition. Note that in all cases, (a,b,) Volcano plots for (a) raw and (b) solvent-normalized experimental activities, colored by solvent: water and TEOA (blue), methanol (orange), and ethanol (green). Note that the y-axis is not normalized by surface area, meaning that variations in height or slope may be attributable to differences in the area of the total reactive interface. (c, d, e, f) Volcano plots for water/TEOA (c), methanol (d), ethanol (e), and solvent-normalized (f) experiments, colored by the most active pure component of each bimetallic composition: Pt (blue), Au (orange), Pd (green), or Cu (red).

2.2 Noble Metals by Solvent

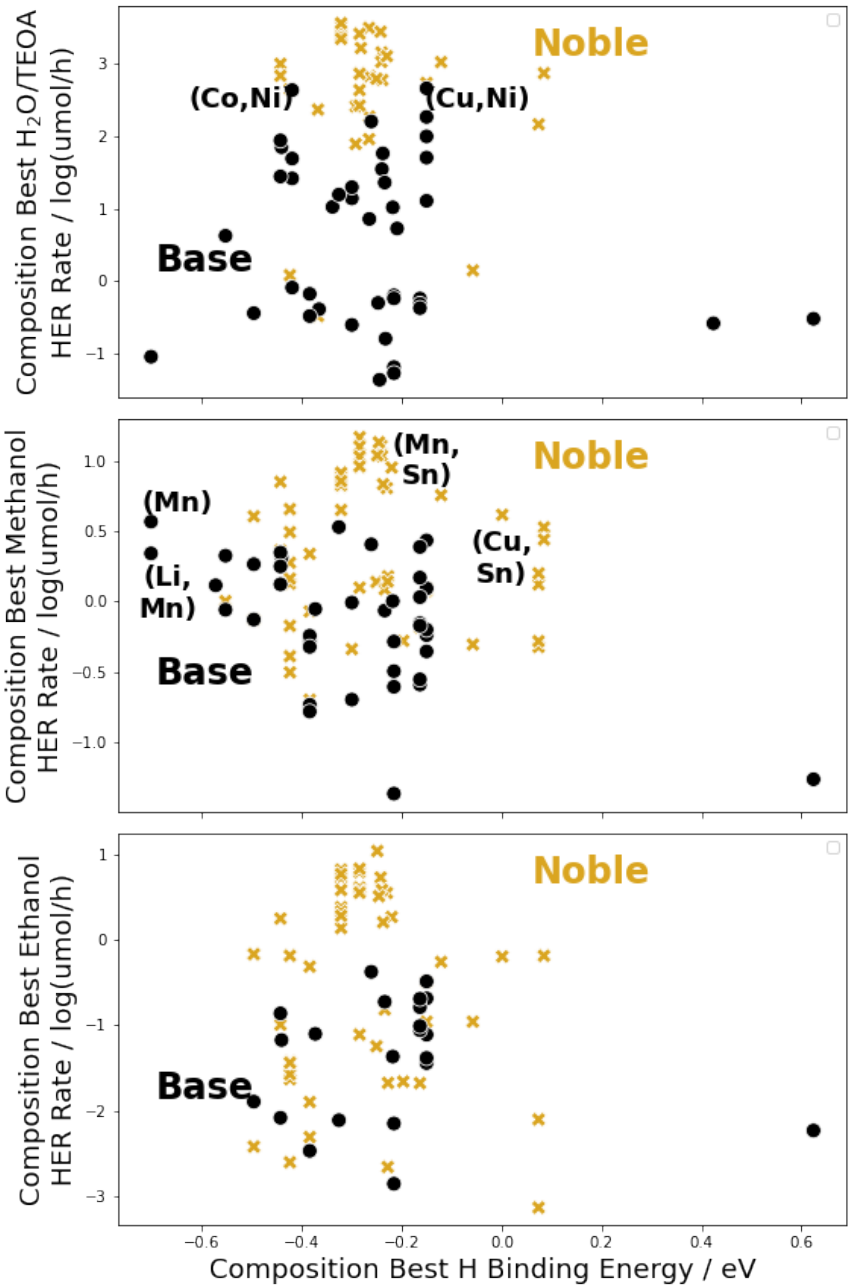

Figure S2: Across all solvent conditions, experiments containing at least one noble metal were more experimentally active by approximately an order of magnitude. Significant positive outliers appear in the Sabatier trend if noble metals are excluded (annotated; note that in many cases the stablest crystal is not bimetallic)

2.3 Multimedia Experimental Activity Comparison

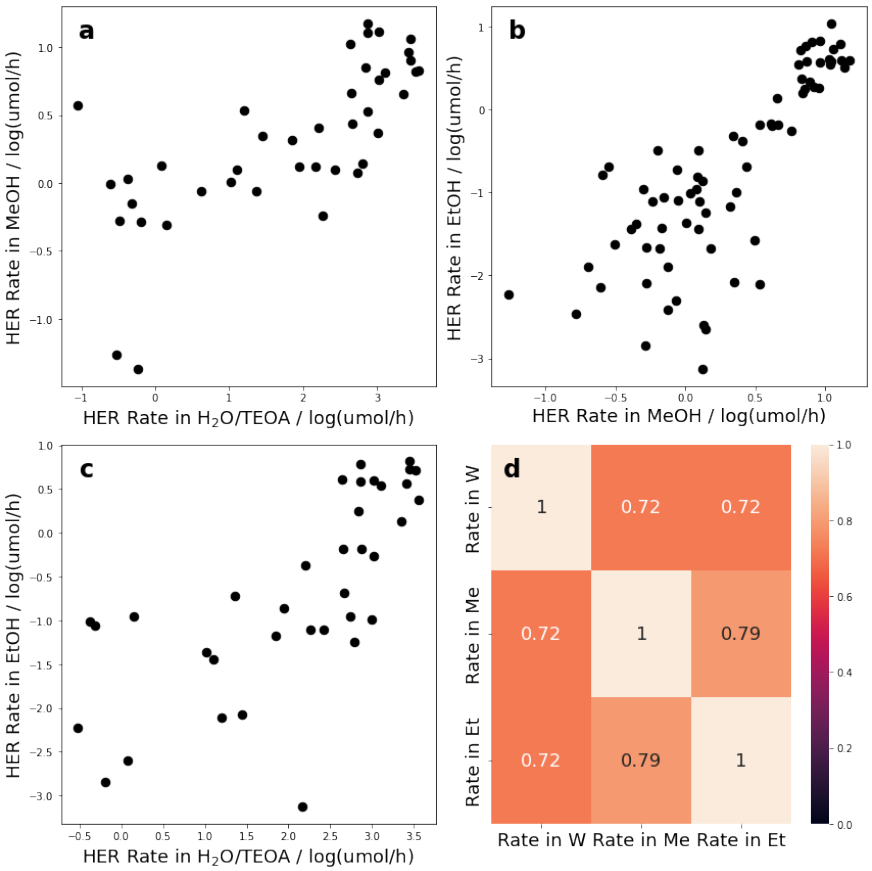

Figure S3: (a,b,c) A comparison of the composition-averaged maximum observed rates of hydrogen evolution for each metal system across different reaction media. (d) The linear correlations of the composition-averaged maximum observed rates of hydrogen evolution for each metal system across different reaction media.

2.4 Gridplot Constructed Using Only System-specific Materials

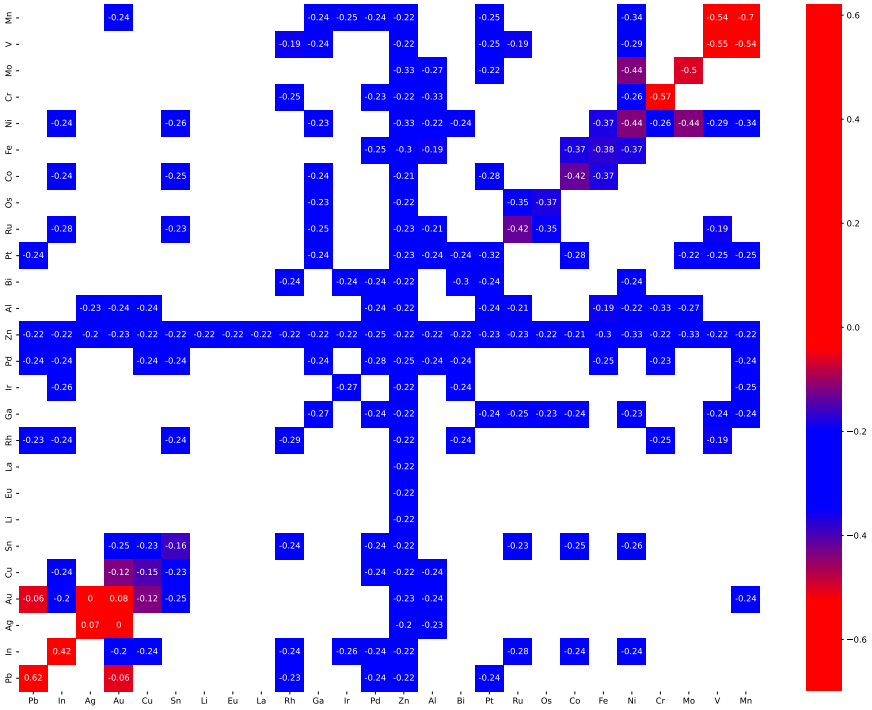

Figure S4: A grid plot of the hydrogen adsorption energy of the surface predicted to be most active. Only metal systems in which a unique compound is predicted to determine activity are shown, for example, Rh/Ir is now empty because the predicted active surface is on a material containing pure Ir.

3 Data and Code Availability

Data and code to run the analyses in this work and reproduce figures are available at www.github.com/Ulissigroup/HER_Manuscript.